Analysis and Design of an integrated LCL-S contactless resonant converter

Wei Gao[1], lixin Jiang[2], Qianhong Chen[1], Xiaoyong Ren[1],Zhiliang Zhang[1],Siu-Chung Wong[3]

[1]College of Automation Engineering
Nanjing University of Aeronautics and Astronautics
Nanjing, China
chenqh@nuaa.edu.cn

[2]NARI TECHNOLOGY CO.,LTD
Nanjing, China
398688442@qq.com

[3]Department of Electronic and Information Engineering
Hong Kong Polytechnic University
Hong Kong, China
enscwong@polyu.edu.hk

***Abstract*—Magnetic integration can be introduced in contactless resonant converter with high-order compensation network, such as LCL and LCC, to reduce the number and volume of the magnetic components. However, the cross couplings among the multi-windings of the integrated contactless transformer will impair the performance of the converter. In this paper, an integrated LCL-S contactless resonant converter is proposed, and the detailed analysis including characteristics of input impedance, voltage gain, input current harmonics and capacitor stress are also given. An improved designing method to achieve a ZPA (zero phase angle) and load-independent voltage gain is presented. Finally, a 1kW prototype is built to verify the theoretical analysis. The analysis and experimental results reveal that LCL compensation with magnetic integration features lower voltage stress across the resonant capacitor.**

Keywords—LCL; contactless resonant converter; Magnetic integration; voltage stress;

I. INTRODUCTION

Magnetic integration has attracted a great deal of interest for its advantages of weight and volume reduction of the magnetics [1-2]. It can also be applied in contactless resonant converter with high-order compensation network, like LCC, LCL, so extra space and magnetic cores for the compensated inductors outside of the coupler can be saved. However, the cross couplings among the multi-windings of the integrated contactless transformer will complicate the analysis and impair the performance of the converter.

Some researches have been made in LCC magnetic integration[3-5]. Paper[3] first proposed integrated LCC compensation topology, which integrates the compensation inductor with main coil and achieves a 6 kW wireless charging system with an efficiency of 95.3%. However the cross couplings among the coils of the integrated transformer, i.e. M_{1f2}, M_{2f1}, M_{f1f2}, as shown in Fig.1, are not considered in the analysis. Although [4] gives detailed analysis considering all cross couplings, the focus of the paper is to reduce the side effect of the cross couplings by improving the coupler design.

This work was supported in part by the National Natural Science Foundation of China (Grant No.51677086), in part by Lite-On Power Electronics Technology Research Fund.

The couplings among coils complicate the analysis and parameter design greatly. Thus a unipolar compensated inductor integrated with bipolar main coils and special placement for the integrated transformer is then presented to further eliminate or minimize the extra coupling effects [5].

The purpose of this paper is to propose an integrated LCL-S (S denotes that the secondary capacitor is series with winding) contactless resonant converter, perform the theoretical analysis considering the effect of cross coupling, and present the parameter design method applicable for integrated LCL-S. The advantages and disadvantages of magnetic integration will be discussed.

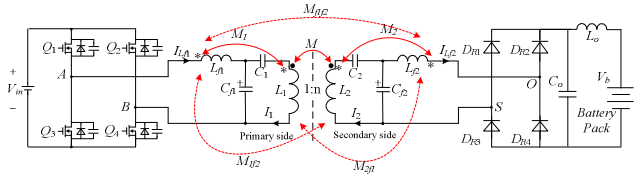

Fig.1. integrated LCC compensation topology

II. EQUIVALENT CIRCUIT OF THE PROPOSED INTEGRATED LCL-S COMPENSATED CONVERTER

A. *Equivalent circuit dervation*

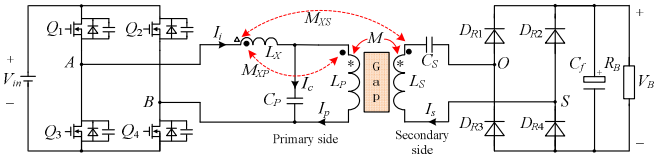

Fig.2. Proposed integrated LCL-S compensated contactless converter

Fig.2 shows the schematic of the proposed magnetic integrated LCL-S topology with positive coupling represented with the reference dots, where M, M_{xs} , M_{xp} are the respective mutual inductances between different windings. Let M_{xs} and M_{xp} be zero, the integrated LCL-S would change to traditional LCL-S. Using fundamental harmonic approximation (FHA), the voltage and current variables are represented by phasors

and the rectifier and the filter can be represented by a resistor R_E (R_E= $8R_B/\pi^2$) [6], as shown in Fig.3 (a).

Based on "M model", the mutual inductance M_{xp} is decoupled, then the circuit is simplified to Fig.3 (b). So the equivalent inductances and capacitor in Fig.3(c) can be rewritten as (1):

$$L_{Xe} = L_X + M_{XP}$$
$$L_{Pe} = L_P + M_{XP} \qquad (1)$$
$$C_{Pe} = C_p / (\omega^2 M_{XP} C_P + 1)$$

Compared with traditional LCL-S contactless topology, we could find that the primary two inductances increase while the equivalent parallel capacitance decreases because of the existence of M_{xp}. In fact , the equivalent negative inductance （$-M_{xp}$） , which is series with C_p , lowers the voltage stress of C_p.

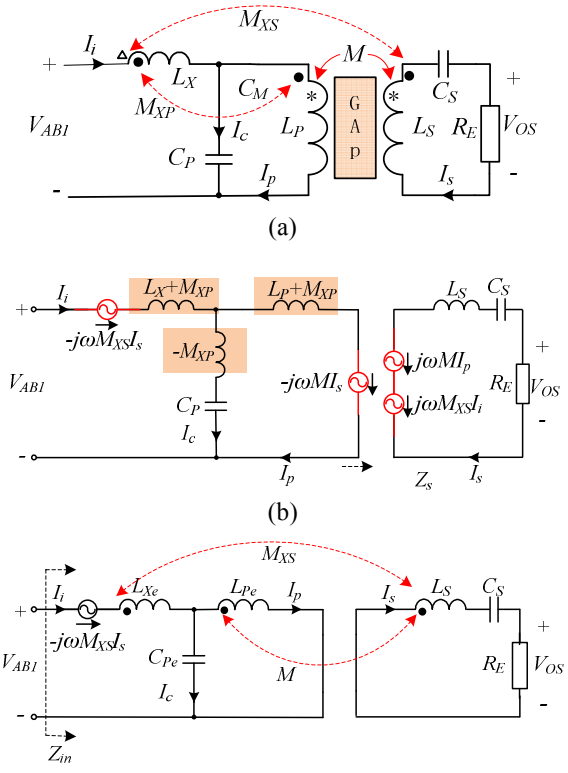

Fig. 3. Equivalent circuit deriving

B. *Compensation design*

Furthermore, by using T model, the circuit in Fig.3(c) is transformed to Fig.4(a), Fig.5(a), where *aj*, *bj*, *cj*, *dj*, *ej*, *fj* are the impendences of different component units respectively(eg. $aj=j\,\omega(L_{xe}-M_{xs})$)

The Y-Δ network transform or Δ-Y network transform can be used to derive the equivalent circuit, as shown in Fig.4(b) and 5 (b).

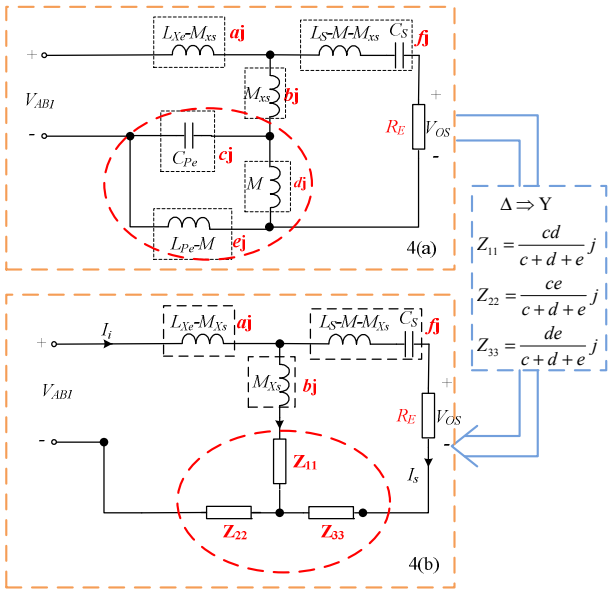

Fig.4. Δ- Y transform : equivalent circuit for constant I_s output

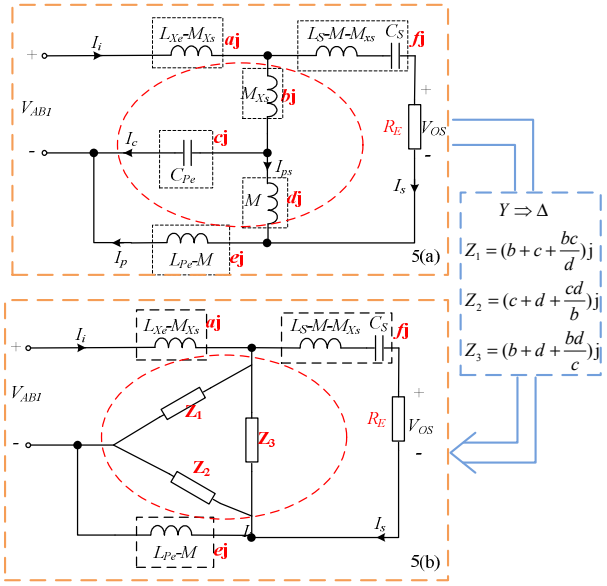

Fig. 5. Y-Δ transform : equivalent circuit for constant V_{os} output

After Y-Δ transform in Fig.4, it is really like a traditional single LCL resonant topology, and the difference is that, here, in T model, the constant output current I_s, independent of R_E ,is just the secondary load current.

Likewise, as can be seen in Fig. 5(b), the equivalent circuit can be treated as an LCL-S T model when taking Z_2 and *ej* as a whole. In order to achieve constant output voltage and ZPA [7], the parameters in Fig.5 (b) should satisfy:

$$aj + Z_1 = 0 \quad aj = (Z_2 // ej) + Z_3 \quad fj + Z_3 = 0 \qquad (2)$$

Substituting Z_1, Z_2, Z_3 given in Fig.5 to (2), we can obtain the solutions (S1, S2):

$$S1:\Rightarrow\begin{cases}\omega_0^2 L_{pe}C_{pe}=1\\ L_{Xe}=L_{pe}\dfrac{M_{Xs}+M}{M}\\ \omega_0^2(L_s-\dfrac{MM_{Xs}}{L_{pe}})C_s=1\end{cases}\qquad S2:\Rightarrow\begin{cases}\omega_0^2(\dfrac{M_{Xs}M}{M_{Xs}+M})C_{pe}=1\\ L_{Xe}=M_{Xs}\\ \omega_0^2(L_s-M-M_{Xs})C_s=1\end{cases}\tag{3}$$

Where ω_0 is the fully compensated angle frequency. From (3), it can be readily found that C_s and L_{Xe} should be redesigned. A series capacitor can be used to adjust the equivalent L_{xe} or L_{pe}. Furthermore, the actual C_p value can be calculated with expression (1). The sub segment analysis of S1 and S2 are similar. Here we choose solution 1(S1) for the following analysis and comparison.

III. CHRACTERISTICS ANALYSIS AND COMPARISONS

Shown in Fig.5, the following analysis are all based on the integrated LCL circuit under compensation S1.When it comes to the analysis of traditional LCL, we only have to let M_{xs} be zero for convenience. It will help us to compare the operation characters of the two kinds of LCL compensation.

A. Voltage gain and Input impedance

From Fig.5 (b), the output voltage gain can be readily obtained in (4). The gain expression of integrated LCL is the same as traditional LCL-S, which indicates the independency of V_{gain} with cross coupling M_{xs}, making the parameters design easier.

Besides, the input impendence derived in (5) shows that the input phase is independent of load, keeping ZPA, which helps to minimize the reactive circular power flow.

$$V_{os}=\frac{V_{AB1}}{j\omega(L_{xe}-M_x)}(j\omega(M_{xs}+M-\frac{M_{xs}*M}{L_{pe}}))$$

$$V_{gain}=\frac{(M_{xs}+M-\dfrac{M_{xs}*M}{L_{pe}})}{L_{pe}(1+\dfrac{M_{xs}}{M})-M_{xs}}=\frac{M}{L_{pe}}=\frac{M}{L_p+M_{xp}}\tag{4}$$

$$Z_{in}=\frac{a^2}{f^2}R_E=(\frac{L_x-M_x}{M_x+M-\dfrac{MM_x}{L_{pe}}})^2R_E$$

$$=(\frac{L_{pe}+L_{pe}\dfrac{M_x}{M}-M_x}{M_x+M-\dfrac{MM_x}{L_{pe}}})^2R_E\tag{5}$$

$$=(\frac{L_{pe}}{M})^2R_E=(\frac{L_p+M_{xp}}{M})^2R_E$$

Tab I gives the result of the compensation parameters between traditional LCL-S and integrated LCL-S. To simplify the experimental validation with the same contactless transformer, a capacitor would be added to be series with primary winding, which compensated the M_{xp} at resonant frequency exactly.

TABLE I . COMPENSATION PARAMETERS OF TRADITIONAL LCL-S AND INTEGRATED LCL-S

	Traditional LCL	Integrated LCL
C_p	$\dfrac{1}{\omega_0^2 L_p}$	$\dfrac{1}{\omega_0^2 L_{pe}}$
C_s	$\dfrac{1}{\omega_0^2 L_s}$	$\dfrac{1}{\omega_0^2(L_s-\dfrac{MM_{Xs}}{L_{pe}})}$
L_x	L_p	$L_{pe}\dfrac{M_{Xs}+M}{M}$
V_{gain}	$\dfrac{M}{L_p}$	$\dfrac{M}{L_{pe}}$
Phase	0	0

B. Capacitor stress and Input Harmonic Current

$$v_{AB}(t)=\frac{4V_{in}}{\pi}\sum_{n=1,3,5...}^{\infty}\frac{\sin(n\omega t)}{n}\tag{6}$$

$$I_{in}=V_{AB1}/Z_{in}=V_{AB1}/((L_p/M)^2R_E)\tag{7}$$

$$I_s=V_{AB1}(M/L_{Pe})/R_E\tag{8}$$

$$I_p=V_{AB1}/j\omega L_{pe}\tag{9}$$

$$I_c=I_{in}-I_p$$
$$=V_{AB1}/((L_{pe}/M)^2R_E)-V_{AB1}/j\omega L_{Pe}\tag{10}$$

It is obvious that equations (6)-(10) don't contain a M_{xs} item, which means that with our proposed compensation method, the primary winding current and resonant capacitor current remain the same as that in traditional LCL-S topology. However, the actual capacitance C_p and C_s are larger than those in traditional LCL-S, so the actual voltage stress of capacitor decreases. On the other hand, as mentioned before, the equivalent negative Inductance, just like a virtual capacitor, have a voltage dividing effect with C_p, which is beneficial to the selection and reliable operation of capacitor.

Though the magnetic integration does not impair the fundamental current, the input high order harmonic current actually changes. Based on the circuit of Fig.6, it is not difficult to derivate the n[th] harmonic current versus frequency. Ratio of the high order harmonic current flowing through the inverters is defined in (10) - (12).

$$I_f=\frac{\sqrt{2}V_{in}}{\pi}\left\{\begin{array}{l}j\omega L_{Xe}+\dfrac{\omega^2M_{XS}^2}{j\omega L_S+(j\omega C_S)^{-1}+R_E}\\ +\dfrac{\omega^2MM_{XS}+(j\omega L_{Pe}+Z_{rp})\left[j\omega L_S+(j\omega C_S)^{-1}+R_E\right]}{\left[j\omega L_S+(j\omega C_S)^{-1}+R_E\right](1-\omega^2L_{Pe}C_{Pe}+j\omega C_{Pe}Z_{rp})}\end{array}\right\}^{-1}\tag{10}$$

$$I_h(n)=\frac{\sqrt{2}V_{in}}{n\pi}\left\{\begin{array}{l}jn\omega L_{Xe}+\dfrac{n^2\omega^2M_{XS}^2}{jn\omega L_S+(jn\omega C_S)^{-1}+R_E}\\ +\dfrac{n^2\omega^2MM_{XS}+(jn\omega L_{Pe}+Z_{rpn})\left[jn\omega L_S+(jn\omega C_S)^{-1}+R_E\right]}{\left[jn\omega L_S+(jn\omega C_S)^{-1}+R_E\right](1-n^2\omega^2L_{Pe}C_{Pe}+jn\omega C_{Pe}Z_{rpn})}\end{array}\right\}^{-1}\tag{11}$$

$$HRI_n(n)=I_h(n)/I_f\tag{12}$$

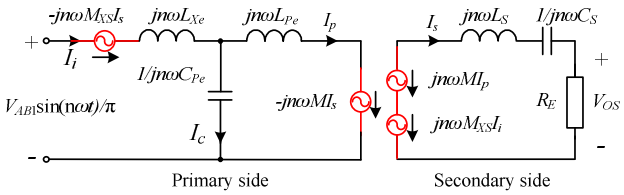

Fig. 6: n harmonic current equivalent circuit

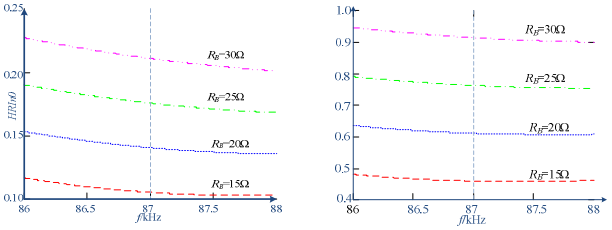

(a) traditional LCL (b) integrated LCL

Fig.7. the ratio of input 3rd harmonic current

With the increase of loads, the $HRI_n(n)$ in (12) decreases in traditional LCL-S and integrated LCL-S, as shown in Fig.7. However, we have to admit that the introduction of magnetic integration increases the inverter harmonic current which is not good for the efficiency improvement.

IV. EXPERIMENTAL RESULTS AND DISCUSSIONS

A 1kW LCL(400_{IN}-125_{OUT}) contactless converter with integrated compensated inductor was built to validate the analysis. Fig.8(a) gives the 2D Ansoft simulation result of a DD contactless transformer. To take full advantage of flux, the resonant inductor is designed to have a similar DD structure and placed close with the primary winding, as shown in Fig.8(b).

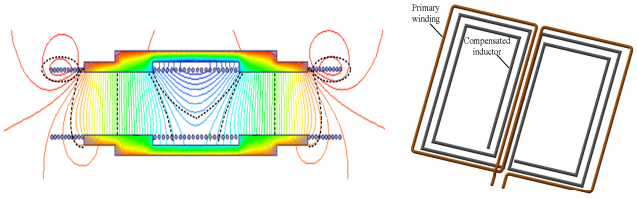

(a)Ansoft flux distribution simulation (b) magnetic integration

Fig.8. integrated LCL design

Fig.9 gives the constructed integrated LCL-S contactless transformer and the parameters can be found in Table II.

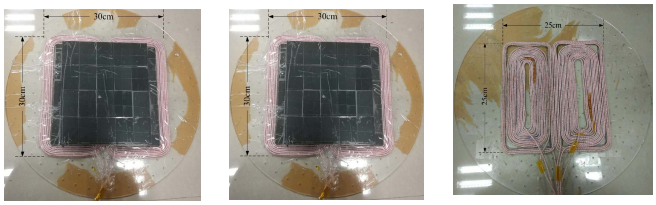

(a) primary winding (b) secondary winding (c) integrated inductor

Fig.9. constructed integrated LCL

TABLE II . PARAMETERS OF CONTACTLESS TRANSFORMER AND COUPLED INDUCTOR

Parameters	Value
Input voltage	400V
Output voltage	125V
Nominal gap	9cm
Rated power	1kW
Transformer dimension	30cm×30cm
Transmitting coil inductance : L_p	302.19uH
pickup coil inductance: L_s	296.7uH
Resonant inductance: L_x	142.00uH
mutual inductance between L_p and L_s :M	100.11uH
mutual inductance between L_p and L_x :M_{xp}	134.89uH
mutual inductance between L_p and L_x :M_{xs}	61.58uH

A. *Voltage gain and system efficiency*

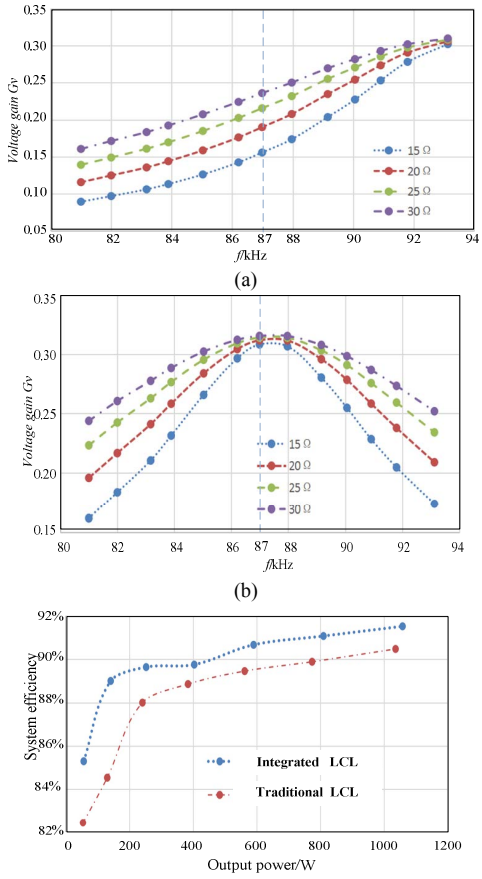

(a)

(b)

(c)

Fig.10: Voltage gain versus frequency (a) C_s without adjustment (b) C_s with adjustment (c) efficiency vs P_o

Fig.10(b) shows that with the new compensation parameters, the voltage gain (DC-DC) is independent of load resistor (R_B) at the resonant frequency. However, if we do not adjust C_s or still use the traditional LCL compensation parameters, the load-independent intersection point moves to a new frequency as shown in Fig.10 (a).

Furthermore, the integrated LCL has a higher efficiency, about 1.5 present, compared with traditional LCL, as shown in

Fig.10(c). The highest efficiency of integrated LCL is 91.5% at full load.

B. *Voltage stress: voltage across C_p*

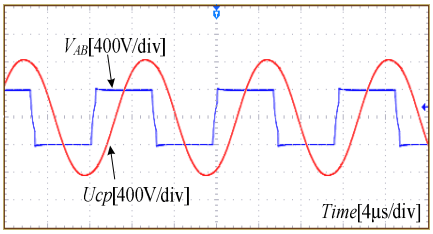

(a) traditional LCL

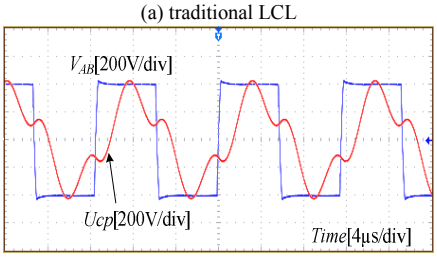

(b) integrated LCL

Fig. 11: Experimental waveforms of inverter voltage and primary resonant capacitor voltage

Fig.11 illustrates the waveforms of inverter voltage and v_{cp} (the voltage across C_p) of the traditional and integrated LCL-S contactless converters at full load. The voltage stress of resonant capacitor decreases by one half, from 800V to 400V, which agrees well with the above analysis.

C. *Harmonic current :inverter current ii*

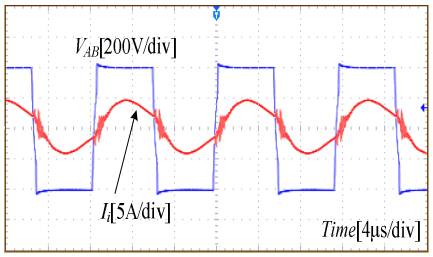

(a) traditional LCL

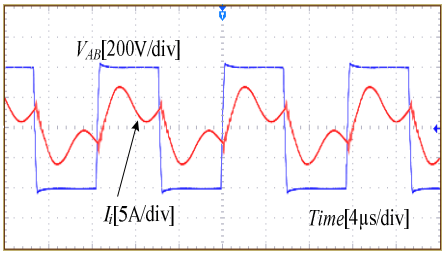

(b) integrated LCL

Fig.12: Experimental waveforms of the inverter voltage, inverter current

Fig.12 gives the waveforms of inverter voltage u_{AB} and inverter current i_i in different LCL-S topologies. It can be readily observed that the inverter current in traditional LCL is in phase with the inverter voltage while in the proposed integrated LCL-S topology the ZPA is not obvious because of the large 3rd harmonic current component in i_i.

V. CONCLUTIONS

This paper proposes a magnetic integrated LCL-S compensated contactless resonant converter. With the primary resonant inductor integrated into the main coil structure, the system becomes more compact. The equivalent decoupled circuit model is derived for the convenience of parameters design and characteristics analysis. A new compensation network design method applicable for integrated LCL is presented so as to achieve a ZPA and constant voltage gain at the resonant frequency. A 1-kW experimental prototype was constructed to verify the correctness of the theoretical analysis. Compared with traditional LCL-S, integrated LCL-S has higher efficiency and lower resonant capacitor voltage stress.

REFERENCES

[1] Qianhong Chen, Ligang Xu, Xiaoyong Ren, Lingling Cao, Xinbo Ruan. A Novel Coupled Inductor for Interleaved Converters[C]. IEEE Annual Applied Power Electronics Conference, 2010, 920-927

[2] Qianhong Chen, Yang Feng, Linquan Zhou, Jian Wang, Xinbo Ruan, "An improved Active Clamp Forward Converter with Integrated Magnetics", IEEE Annual Power Electronics Specialists Conference, v 1, 2007, p 377-382)

[3] W. Li, H. Zhao, S. Li, J. Deng, T. Kan, and C. C. Mi, "Integrated LCC Compensation Topology for Wireless Charger in Electric and Plug-in Electric Vehicles," IEEE Transactions on Industrial Electronics, vol. 62, no. 7, pp. 4215–4225, Jul. 2015.

[4] J. Deng, W. Li, T. D. Nguyen, S. Li, and C. C. Mi, "Compact and Efficient Bipolar Coupler for Wireless Power Chargers: Design and Analysis," IEEE Transactions on Power Electronics, vol. 30, no. 11, pp. 6130–6140, Nov. 2015.

[5] T. Kan, T.-D. Nguyen, J. C. White, R. K. Malhan, and C. C. Mi, "A New Integration Method for an Electric Vehicle Wireless Charging System Using LCC Compensation Topology: Analysis and Design," IEEE Transactions on Power Electronics, vol. 32, no. 2, pp. 1638–1650, Feb. 2017.

[6] W. Zhang, S. C. Wong, C. K. Tse, and Q. H. Chen, "Analysis and comparison of secondary series and parallel compensated inductive power transfer systems operating for optimal efficiency and load independent voltage-transfer ratio," IEEE Trans. on Power Electron., vol. 29, no. 6, pp. 2979-2990, June 2014.

[7] W. Zhang and C. C. Mi, "Compensation Topologies of High-Power Wireless Power Transfer Systems," IEEE Transactions on Vehicular Technology, vol. 65, no. 6, pp. 4768–4778, Jun. 2016.